

Boosted Self-Interacting Dark Matter and XENON1T Excess

Debasish Borah,^{1,*} Manoranjan Dutta,^{2,†} Satyabrata Mahapatra,^{2,‡} and Narendra Sahu^{2,§}

¹*Department of Physics, Indian Institute of Technology Guwahati, Assam 781039, India*

²*Department of Physics, Indian Institute of Technology Hyderabad,
Kandi, Sangareddy 502285, Telangana, India*

Abstract

We propose a self-interacting boosted dark matter (DM) scenario as a possible origin of the recently reported excess of electron recoil events by the XENON1T experiment. The Standard Model has been extended with two vector-like fermion singlets charged under a dark $U(1)_D$ gauge symmetry to describe the dark sector. While the presence of light vector boson mediator leads to sufficient DM self-interactions to address the small scale issues of cold dark matter, the model with sub-GeV scale DM can explain the XENON1T excess via scattering of boosted DM component with electrons at the detector. Strong annihilation of DM into the light mediator leads to suppressed thermal relic. A hybrid setup of dark freeze-out and non-thermal contribution from the late decay of a scalar can lead to correct relic abundance. All these requirements leave a very tiny parameter space for sub-GeV DM keeping the model very predictive for near future experiments.

*Electronic address: dborah@iitg.ac.in

†Electronic address: ph18resch11007@iith.ac.in

‡Electronic address: ph18resch11001@iith.ac.in

§Electronic address: nsahu@phy.iith.ac.in

I. INTRODUCTION

There exist ample evidences towards the presence of Dark Matter (DM), a non-luminous, non-baryonic form of matter in the present universe, which constitutes a very significant portion of galaxies, clusters and the whole universe [1, 2]. Data from satellite-borne experiments like Planck and WMAP, which measure anisotropies in the the cosmic microwave background (CMB) very precisely, predict the amount of DM in the present universe to be around one-fourth (26.8%) of the current energy density of the universe. In terms of density parameter Ω_{DM} and $h = \text{Hubble Parameter}/(100 \text{ km s}^{-1}\text{Mpc}^{-1})$, the present abundance of DM is conventionally reported as [2]: $\Omega_{\text{DM}}h^2 = 0.120 \pm 0.001$ at 68% CL. Similar evidences exist for DM in galactic and cluster scales as well, collected over a long period of time since 1930's [3–5]. It should be noted that the estimate of present DM abundance is done by Planck relying upon the standard model of cosmology or Λ CDM model which has been very successful in describing our universe at large scale ($\geq \mathcal{O}(\text{Mpc})$). Here CDM refers to cold dark matter while Λ denotes the cosmological constant or dark energy. CDM is a pressure-less or collision-less fluid which acts like a seed for structure formation by providing the required gravitational potential well for ordinary matter to collapse and form structures. Since none of the standard model (SM) particles mimic the properties that a DM particle expected to have, several beyond standard model (BSM) scenarios have been proposed, out of which the weakly interacting massive particle (WIMP) paradigm has been the most widely studied one. In this framework, a WIMP candidate having interactions and mass in the typical electroweak regime, naturally satisfies the correct DM relic abundance—a remarkable coincidence often referred to as the *WIMP Miracle* [6]. A recent review of WIMP type models can be found in [7].

While Λ CDM is in excellent agreement with large scale structure of the universe, yet at small scales, it faces challenges from observations like too-big-to-fail, missing satellite and core-cusp problems. For recent reviews of these issues and possible solutions, refer to [8, 9]. One interesting solution to this puzzle was proposed by Spergel and Steinhardt [10] where they considered self-interacting dark matter (SIDM) as an alternative to collision-less CDM¹. The advantage of SIDM is that it solves the problems at small scales, while

¹ See [11] for earlier studies.

reproduces the CDM halos at large radii, thus consistent with observations. This is simply because of the fact that self-interacting scattering rate is proportional to DM density. The required self-interaction rate is often quantified as a ratio of cross section to DM mass as $\sigma/m \sim 1 \text{ cm}^2/\text{g} \approx 2 \times 10^{-24} \text{ cm}^2/\text{GeV}$ [12–17]. Such self-interacting cross sections can be naturally realised in models with a very light mediator. For such a scenario, self-interactions can be shown to be stronger for smaller DM velocities such that it can have large impact on small scale structures while being consistent with usual CDM predictions at larger scales [12–15, 18–21]. From particle physics point of view, such self-interactions can be naturally realised in Abelian gauge extensions of the SM. The dark sector can not be completely hidden and there should be some coupling of the mediator with SM particles as well, which can ensure that DM and SM sectors were in thermal equilibrium in the early universe. The same coupling can also be probed at DM direct detection experiments as well [22, 23], and indeed one such possibility is the topic of this work.

DM with light mediators have also received attention very recently after XENON1T collaboration published their latest results in June 2020 where they have reported the observation of an excess of electron recoil events over the background in the recoil energy E_r in a range 1-7 keV, peaked around 2.4 keV[24]. While the excess can be explained by solar axions at 3.5σ significance or neutrinos with magnetic moment at 3.2σ significance both these interpretations face stringent stellar cooling bounds. While there is also room for possible tritium backgrounds in the detector, which XENON1T collaboration has neither confirmed nor ruled out so far, there have been several interesting new physics proposals in the literature. For example, see [25–45] and references therein. The DM interpretations out of these examples, typically have a light mediator via which DM interacts with electrons. The recoil can occur either due to light boosted DM or inelastic up or down-scattering [32–41, 45–55, 55–58]. For further detection prospects of such boosted DM in different experiments, see [59–63].

Thus we noticed that in a class of models, the DM interpretation of XENON1T excess as well as SIDM phenomenology rely on light mediators. This motivates us to propose a common platform to demonstrate that the self-interaction of DM arising via light mediators in such models can also give rise the observed XENON1T excess. In other words, the proposed scenario provides a unique way of probing the parameter space of SIDM at direct DM search experiments like XENON1T. There have been two such attempts so far trying to

address XENON1T excess within SIDM framework. In our earlier work [45], we considered inelastic SIDM scattering off electrons while in another recent work [64] considered the decay of an excited state into DM and a very light sub-eV vector mediator leading to a dark photo-electric effect. In the present work, we consider the possibility of boosted SIDM where heavier DM annihilates into the lighter one followed by scattering of the latter off electrons at the XENON1T detector². To be more specific, we consider a dark sector consisting of two vector-like fermion singlets charged under an additional $U(1)_D$ gauge symmetry. The corresponding massive vector boson Z' which mediates DM self-interactions is considered to be light (order of magnitude lighter than DM mass) to give rise to the required DM self-interactions at different scales. The same Z' gauge boson can also mix with $U(1)_Y$ gauge boson to provide a unique portal for detecting the DM at direct search experiments including the electron recoil events at XENON1T detector. We first find the DM parameter space consistent with velocity dependent self-interaction rates explaining the astrophysical data at the scale of clusters, galaxies and dwarf galaxies. We then confront the SIDM parameter space with the observed XENON1T electron excess while being consistent with other experimental bounds. We show that these two requirements make pure thermal relic DM insufficient to produce the observed relic and therefore we consider a hybrid setup where both freeze-out and freeze-in mechanisms can play non-trivial roles in generating DM relic. As we discuss in the upcoming sections, the late time decay of a singlet scalar into DM helps in generating correct DM relic in such a hybrid setup.

This paper is organised as follows. In section II, we present our model followed by the analysis for dark matter self-interaction in section III. In section IV, we discuss production mechanism of DM in the early universe. The possible origin of XENON1T excess in our model via boosted DM scenario has been discussed in section V. We finally summarise our results and conclude in section VI.

II. THE MODEL

The matter particle content of the model apart from the SM ones are shown in table I. The Lagrangian with the interactions relevant for determining the DM abundance in the

² Only boosted DM interpretation of XENON1T excess in the context of different models have been discussed in [27–30, 54, 55, 55–58]. See [65, 66] for earlier works on this possibility.

| Fields | | $SU(3)_c \otimes SU(2)_L \otimes U(1)_Y \otimes U(1)_D$ | | | |
|---------|----------|---|---|---|----|
| Fermion | χ_1 | 1 | 1 | 0 | -1 |
| | χ_2 | 1 | 1 | 0 | -1 |
| Scalars | Φ_1 | 1 | 1 | 0 | 0 |
| | Φ_2 | 1 | 1 | 0 | 2 |

TABLE I: BSM fields and their transformations under the gauge symmetry.

considered scenario is given by

$$\mathcal{L}_{\text{DM}} \supset i \bar{\chi}_i \gamma^\mu D_\mu \chi_i - m_i \bar{\chi}_i \chi_i - y_i \bar{\chi}_i \chi_i \Phi_1 - y'_i \bar{\chi}_i^c \chi_i \Phi_2 + \frac{\epsilon}{2} B^{\alpha\beta} Y_{\alpha\beta} \quad (1)$$

where $D_\mu = \partial_\mu + ig' Z'_\mu$ and $B^{\alpha\beta}, Y_{\alpha\beta}$ are the field strength tensors of $U(1)_D, U(1)_Y$ respectively and ϵ is the kinetic mixing between them. The subscript $i = 1, 2$ corresponds to two different singlet fermions. We consider the mass and couplings of two singlet fermions in their diagonal mass basis. The singlet scalars Φ_1, Φ_2 are assumed not to acquire any vacuum expectation values (VEV). The $U(1)_D$ gauge boson can acquire non-zero mass due to spontaneous symmetry breaking induced by another scalar or Stueckelburg mechanism without affecting rest of the analysis discussed in this work. For desired DM phenomenology, we assume $y_{1,2} \ll 1$ and χ_1 to be slightly heavier than χ_2 so that the former can annihilate into the latter with a large cross-section: $\sigma(\chi_1 \chi_1 \rightarrow \chi_2 \chi_2) \approx 10^{-24} \text{cm}^2$, providing a necessary flux of boosted χ_2 to explain XENON-1T excess. Note that such a large value of $\sigma(\chi_1 \chi_1 \rightarrow \chi_2 \chi_2)$ can be achieved through resonant annihilation of χ_1 to χ_2 via Φ_2 exchange.

The Lagrangian involving singlet scalars can be written as

$$\begin{aligned} \mathcal{L}_\Phi \supset & \frac{1}{2} (\partial_\mu \Phi_1)^\dagger (\partial^\mu \Phi_1) - \frac{1}{2} m_{\phi_1}^2 \Phi_1^2 - \lambda_{\phi_1} \Phi_1^4 + (D_\mu \Phi_2)^\dagger (D^\mu \Phi_2) - m_{\phi_2}^2 \Phi_2^\dagger \Phi_2 - \lambda_{\phi_2} (\Phi_2^\dagger \Phi_2)^2 \\ & - \lambda_{1H} (\Phi_1^2) (H^\dagger H) - \lambda_{2H} (\Phi_2^\dagger \Phi_2) (H^\dagger H) - \lambda_{12} (\Phi_1^\dagger \Phi_1) (\Phi_2^\dagger \Phi_2) \end{aligned} \quad (2)$$

where $D_\mu \Phi_2 = \partial_\mu \Phi_2 + i2g' Z'_\mu \Phi_2$. If an additional singlet scalar VEV (u) gives rise to $U(1)_D$ gauge boson mass $M_{Z'} = g'u$ and also breaks the $U(1)_D$ spontaneously down to a remnant Z_2 symmetry under which $\chi_{1,2}$ are odd while all other fields are even, the stability of $\chi_{1,2}$ is ensured making them the viable DM candidates. Although the heavier DM can decay into the lighter one via singlet scalar coupling, we are considering such off-diagonal Yukawa couplings to be negligible.

III. DARK MATTER SELF-INTERACTION

The dark sector particles have elastic self-scattering through Z' -mediated t-channel processes, thanks to the presence of terms like $g' Z'_\mu \bar{\chi}_i \gamma^\mu \chi_i$ in the model Lagrangian given by Eqn. (1). As we will see later, both χ_1 and χ_2 contribute to the present relic abundance of DM. Since their masses are very close to each other to give rise to the required boost factor and both have same gauge interactions, they contribute almost equally to the present DM abundance. Therefore, it suffices to discuss their self-interactions considering it to be a single component DM only. In order to explain small-scale astrophysical observations, the typical DM elastic scattering cross-section should be $\sigma \sim 1 \text{ cm}^2 (\frac{m_{\text{DM}}}{g}) \approx 2 \times 10^{-24} \text{ cm}^2 (\frac{m_{\text{DM}}}{\text{GeV}})$, which is many orders of magnitude larger than the typical weak-scale cross-section ($\sigma \sim 10^{-36} \text{ cm}^2$), suggesting the existence of a dark mediator much lighter than weak scale for DM mass around the electroweak ballpark. So we consider the $U(1)_D$ gauge boson of our model to be much lighter (order of magnitude lighter) than DM so that the non-relativistic DM scattering can be described by a Yukawa potential,

$$V(r) = \pm \frac{\alpha'}{r} e^{-M_{Z'} r} \quad (3)$$

where the $+$ ($-$) sign denotes repulsive (attractive) potential and $\alpha' = g'^2/4\pi$ is the dark fine structure constant. While $\chi_i \bar{\chi}_i$ interaction is attractive, $\chi_i \chi_i$ and $\bar{\chi}_i \bar{\chi}_i$ are repulsive. We consider nearly degenerate masses for χ_1 and χ_2 , hence $m_{\chi_1} \approx m_{\chi_2} = m_{DM}$. To capture the relevant physics of forward scattering divergence for the self-interaction we define the transfer cross-section σ_T as [8, 13, 21]:

$$\sigma_T = \int d\Omega (1 - \cos \theta) \frac{d\sigma}{d\Omega} \quad (4)$$

In the Born Limit ($\alpha' m_{DM}/M_{Z'} \ll 1$), for both attractive as well as repulsive potentials, the transfer cross-section is:

$$\sigma_T^{\text{Born}} = \frac{8\pi\alpha'^2}{m_{DM}^2 v^4} \left(\ln(1 + m_{DM}^2 v^2 / M_{Z'}^2) - \frac{m_{DM}^2 v^2}{M_{Z'}^2 + m_{DM}^2 v^2} \right). \quad (5)$$

Outside the Born regime ($\alpha' m_{DM}/M_{Z'} \gtrsim 1$), we have two distinct regions. In the classical limit ($m_{DM} v / M_{Z'} \gtrsim 1$), the solutions for an attractive potential is given by [21, 67, 68]:

$$\sigma_T^{\text{classical}}(\text{attractive}) = \begin{cases} \frac{4\pi}{M_{Z'}^2} \beta^2 \ln(1 + \beta^{-1}) & \beta \lesssim 10^{-1} \\ \frac{8\pi}{M_{Z'}^2} \beta^2 / (1 + 1.5\beta^{1.65}) & 10^{-1} \lesssim \beta \lesssim 10^3 \\ \frac{\pi}{M_{Z'}^2} (\ln \beta + 1 - \frac{1}{2} \ln^{-1} \beta) & \beta \gtrsim 10^3, \end{cases} \quad (6)$$

and for the repulsive case;

$$\sigma_T^{\text{classical}}(\text{repulsive}) = \begin{cases} \frac{2\pi}{M_{Z'}^2} \beta^2 \ln(1 + \beta^{-2}) & \beta \lesssim 1 \\ \frac{\pi}{M_{Z'}^2} (\ln 2\beta^2 - \ln \ln 2\beta)^2 & \beta \gtrsim 1 \end{cases} \quad (7)$$

where $\beta = 2\alpha' M_{Z'}/(m_{DM}v^2)$.

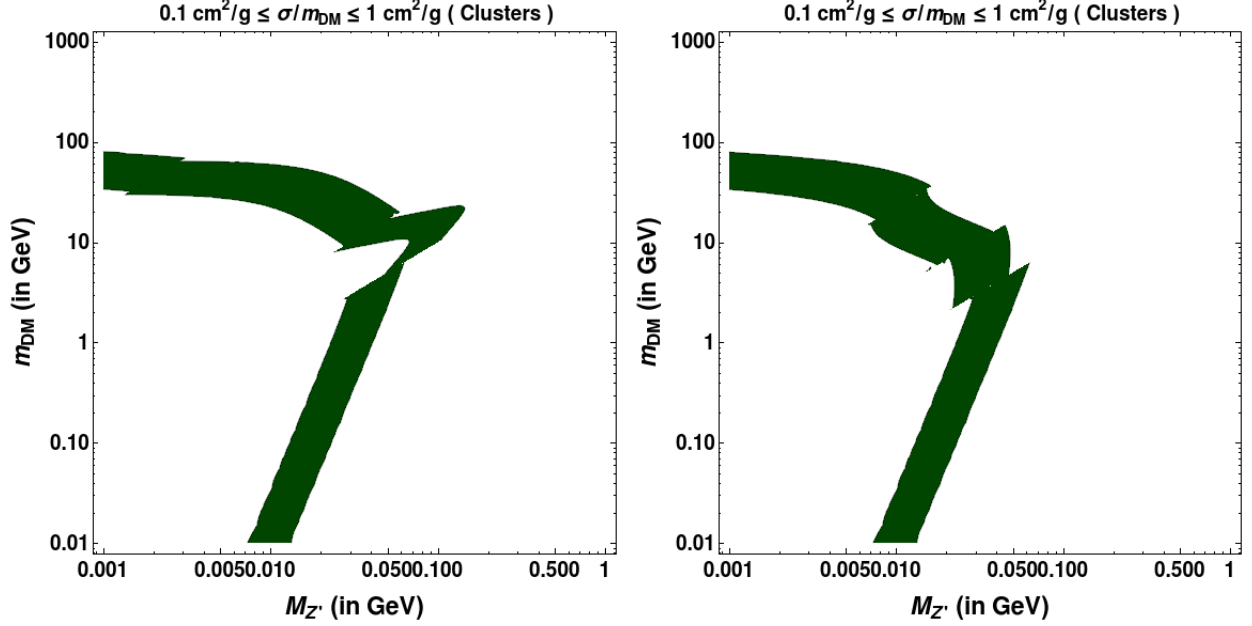


FIG. 1: Parameter space giving rise to attractive (left panel) and repulsive (right panel) self-interaction cross-section in the range $0.1 - 1 \text{ cm}^2/\text{g}$ for clusters ($v \sim 1000 \text{ km/s}$).

Outside the classical regime ($\alpha' m_{DM}/M_{Z'} \gtrsim 1, m_{DM}v/M_{Z'} \lesssim 1$), we get the resonant regime the cross-section is largely dominated by s-wave scattering. Here quantum mechanical resonances appear in σ_T corresponding to (quasi-)bound states in the potential. In this regime, an analytical formula for σ_T does not exist, and one has to solve the Schrodinger equation by partial wave analysis. Here we use the non-perturbative results for s-wave ($l=0$) scattering within the resonant regime obtained by approximating the Yukawa potential to be a Hulthen potential ($V(r) = \pm \frac{\alpha' \delta e^{-\delta r}}{1 - e^{-\delta r}}$) which is given by [21]:

$$\sigma_T^{\text{Hulthen}} = \frac{16\pi \sin^2 \delta_0}{m_{DM}^2 v^2} \quad (8)$$

where $l=0$ phase shift is given in terms of the Γ functions as :

$$\delta_0 = \arg \left(\frac{i\Gamma\left(\frac{im_{DM}v}{kM_{Z'}}\right)}{\Gamma(\lambda_+)\Gamma(\lambda_-)} \right), \quad \lambda_{\pm} = \begin{cases} 1 + \frac{im_{DM}v}{2kM_{Z'}} \pm \sqrt{\frac{\alpha' m_{DM}}{kM_{Z'}} - \frac{m_{DM}^2 v^2}{4k^2 M_{Z'}^2}} & \text{Attractive} \\ 1 + \frac{im_{DM}v}{2kM_{Z'}} \pm i\sqrt{\frac{\alpha' m_{DM}}{kM_{Z'}} + \frac{m_{DM}^2 v^2}{4k^2 M_{Z'}^2}} & \text{Repulsive} \end{cases} \quad (9)$$

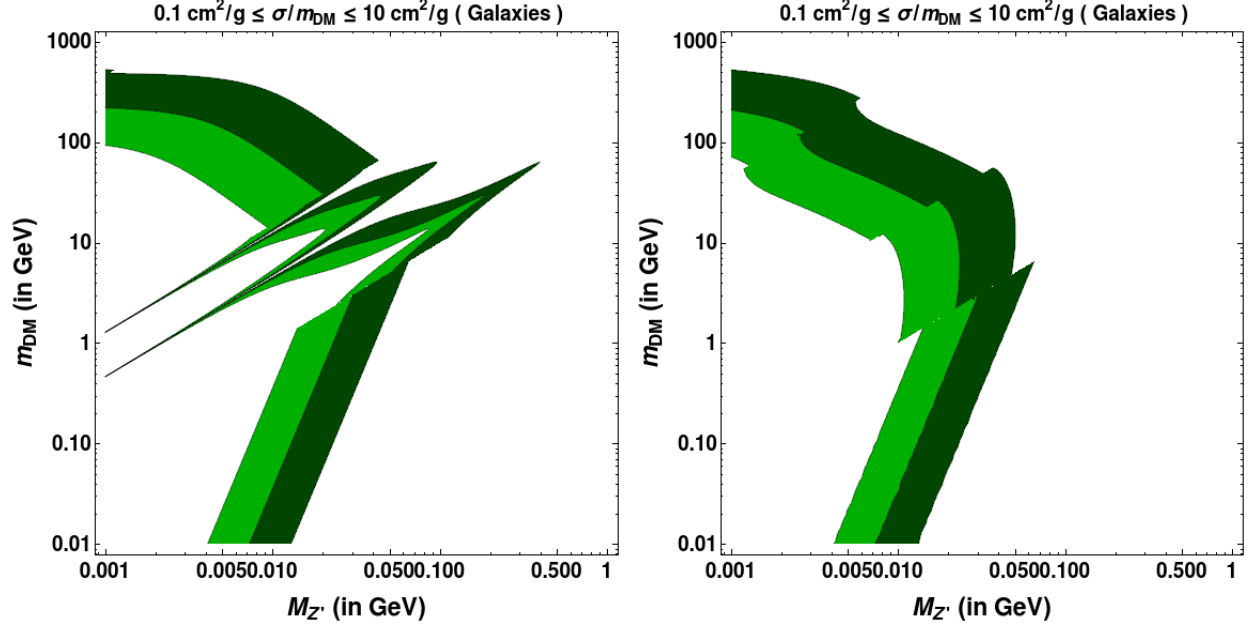


FIG. 2: Parameter space giving rise to attractive (left panel) and repulsive (right panel) self-interaction cross-section in the range $0.1 - 10 \text{ cm}^2/\text{g}$ for galaxies ($v \sim 200 \text{ km/s}$). Green colour represents regions of parameter space where $1 \text{ cm}^2/\text{g} < \sigma/m_{\text{DM}} < 10 \text{ cm}^2/\text{g}$; Dark green colour represents regions of parameter space where $0.1 \text{ cm}^2/\text{g} < \sigma/m_{\text{DM}} < 1 \text{ cm}^2/\text{g}$.

and $k \approx 1.6$ is a dimensionless number. The differential cross-section is $d\sigma/d\Omega = \sigma_T/(4\pi)$.

Using these self-interaction cross sections and using the required σ/m_{DM} from astrophysical observations at different scales, we constrain the parameter space of the model in terms of DM ($\chi_{1,2}$) and mediator Z' masses. In Fig. 1,2,3, we show the allowed parameter space in DM mass versus Z' mass plane which gives rise to the required DM self-interaction cross-section (σ/m_{DM}) in the range $\sigma \in 0.1 - 1 \text{ cm}^2/\text{g}$ for clusters ($v \sim 1000 \text{ km/s}$), $\sigma \in 0.1 - 10 \text{ cm}^2/\text{g}$ for galaxies ($v \sim 200 \text{ km/s}$) and $\sigma \in 0.1 - 100 \text{ cm}^2/\text{g}$ dwarf galaxies ($v \sim 10 \text{ km/s}$) respectively. Because of the light vector mediator, here we can have both attractive and repulsive interactions unlike in the case with a scalar mediator where the interactions are purely attractive. The sharp spikes in the left panels of Fig. 2,3 are the patterns of quantum mechanical resonances and antiresonances for the attractive potential case which is absent for the repulsive case, shown on the right panels. It is clear that the resonant regime corresponds to a large region of parameter space. These features are more prominent for the galactic and dwarf galactic scales where DM has smaller velocities. This is due to the fact that for a fixed α' , the condition $m_{\text{DM}}v/M_{Z'} < 1$ governs the onset of quantum me-

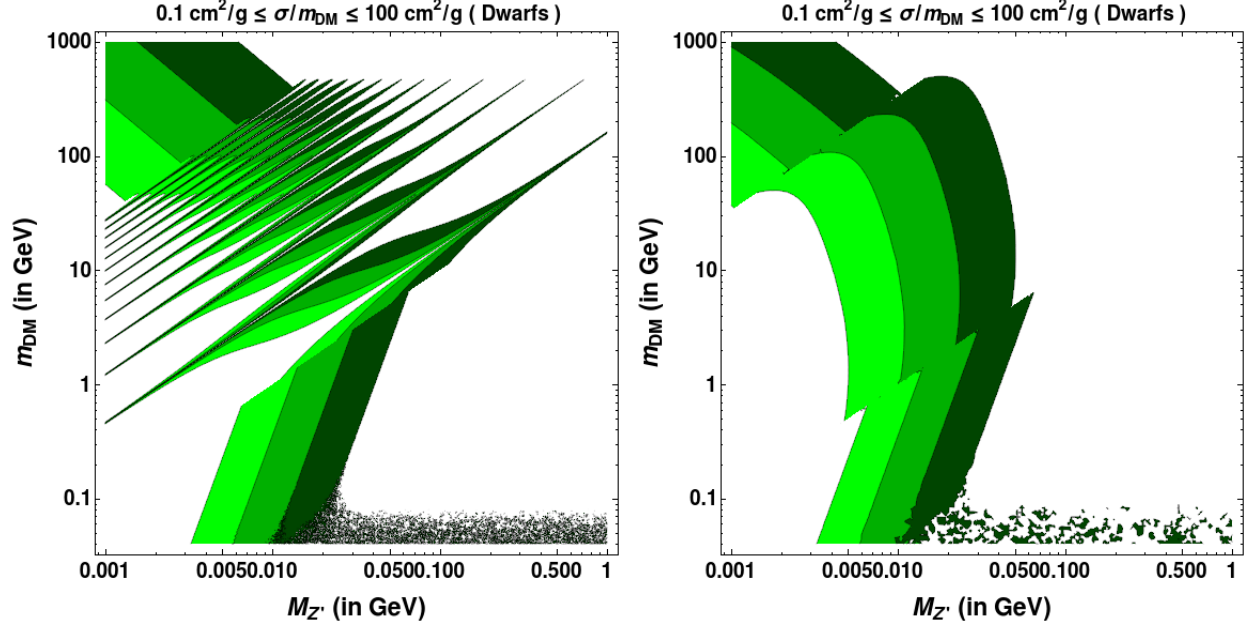


FIG. 3: Parameter space giving rise to attractive (left panel) and repulsive (right panel) self-interaction cross-section $0.1 - 100 \text{ cm}^2/\text{g}$ for dwarfs ($v \sim 10 \text{ km/s}$). Lime green colour represents regions of parameter space where $10 \text{ cm}^2/\text{g} < \sigma/m_{\text{DM}} < 100 \text{ cm}^2/\text{g}$; Green colour represents regions of parameter space where $1 \text{ cm}^2/\text{g} < \sigma/m_{\text{DM}} < 10 \text{ cm}^2/\text{g}$; Dark green colour represents regions of parameter space where $0.1 \text{ cm}^2/\text{g} < \sigma/m_{\text{DM}} < 1 \text{ cm}^2/\text{g}$.

chanical and non-perturbative effects. Clearly a wide range of DM mass is allowed from the self-interaction requirements but mediator mass is constrained within one or two orders of magnitudes (except in the resonance regimes) from both cosmological and astrophysical requirements. We will finally compare these regions of parameter space of GeV scale DM mass in the context of XENON1T excess and other phenomenological constraints.

The self-interaction cross section per unit DM mass as a function of average collision velocity is shown in figure 4 as measured from astrophysical data. The data includes measurements from dwarfs (orange), LSBs (blue) and clusters (green) [19, 69]. The red dashed curve corresponds to the velocity-dependent cross section calculated from our model for a particular set of benchmark values (i.e $m_{\text{DM}} = 4.5 \text{ GeV}$, $M_{Z'} = 10 \text{ MeV}$ and $\alpha' = 0.002$) allowed from all relevant phenomenological constraints. It is clear from the figure that the model proposed here can explain the astrophysical observation of velocity dependent DM self-interaction appreciably well.

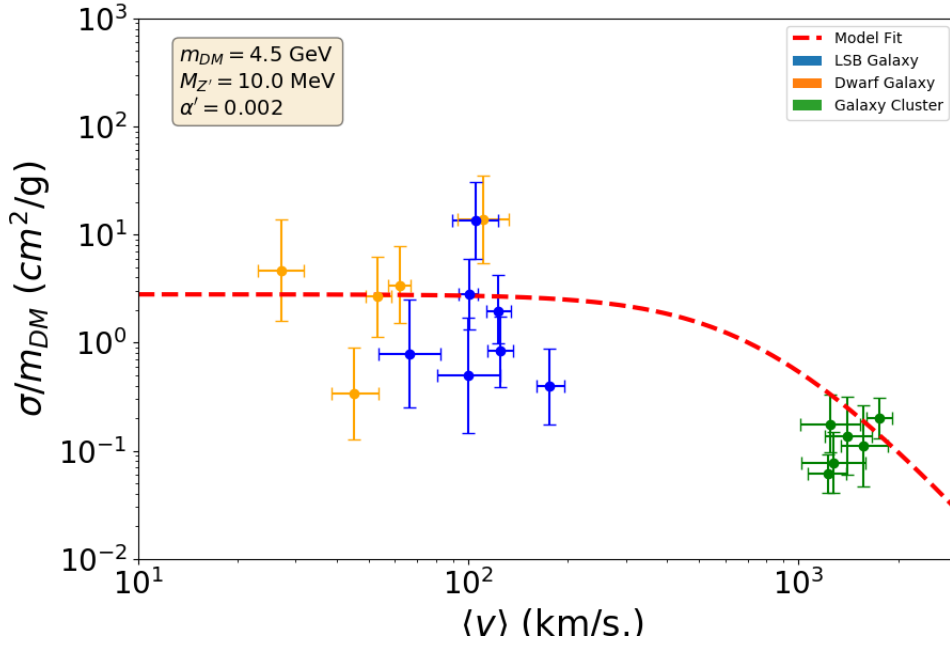


FIG. 4: The self-interaction cross section per unit mass of DM as a function of average collision velocity.

IV. PRODUCTION OF DARK MATTER

There exists several ways of SIDM production in the literature [70–76]. We adopt a minimalistic approach here by first considering the usual $2 \leftrightarrow 2$ vector portal interactions between DM and SM sectors. While DM can interact with itself via Z' as well as singlet scalar interactions, we consider the vector portal to be dominant due to light Z' and sizeable g' . On the other hand, DM can interact with the SM bath only via kinetic mixing of neutral vector bosons or singlet scalar mixing with the SM Higgs boson. However, we ignore the DM-SM interaction via scalar portal in this work and try to constrain the gauge portal maximally from all relevant phenomenology. Thus, the dominant number changing processes for DM are the ones shown in Fig. 5. While DM-SM interactions via kinetic mixing is responsible for production of DM from the thermal bath, the dark sector interactions can be important to decide final thermal abundance of DM. Since from SIDM point of view we consider heavier DM mass compared to the mediator $m_{DM} > M_{Z'}$, DM can have a large annihilation cross section to Z' affecting its relic abundance. For example, the thermal averaged cross section

for the t-channel process $\chi_i \chi_i \rightarrow Z' Z'$ shown in the left panel of Fig. 5 is

$$\langle \sigma v \rangle \sim \frac{\pi \alpha'^2}{m_{\text{DM}}^2} \quad (10)$$

where m_{DM} denotes the masses of $\chi_{1,2}$ which are very close to each other. For typical gauge coupling and DM mass of our interest namely, $\alpha' \sim 0.001$, $m_{\text{DM}} \sim 0.1$ GeV, this leads to a cross section which is at least two order of magnitudes larger compared to the typical annihilation cross section of thermal DM. This reduces the relic abundance by same order of magnitudes, as seen from Fig. 6 showing the comoving number density of DM, assuming it to be a purely thermal relic. While we have assumed the DM to be in equilibrium initially, it need not be so if the kinetic mixing parameter is very small. In fact, we need to consider very small kinetic mixing ($\sim 10^{-7}$) to realise the XENON1T excess. To check, whether DM-SM interactions can reach equilibrium in the early universe, we compare the rates of different annihilation processes. For numerical analysis, the model has been implemented in LanHEP [77] and CalcHEP [78].

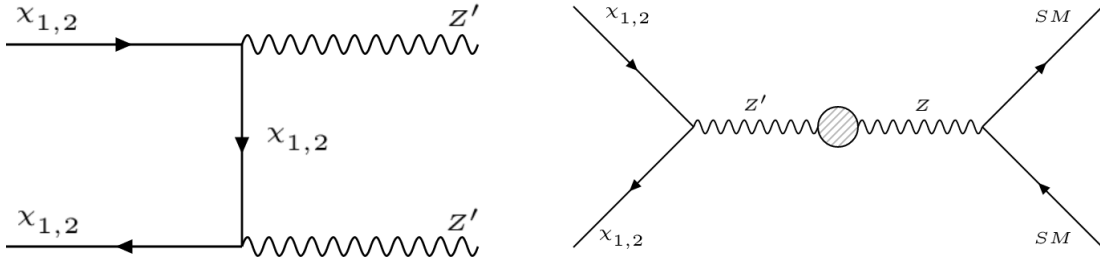


FIG. 5: Feynman diagrams for dominant number changing processes of DM.

From Fig 7, it is evident that the Dark sector interactions are in equilibrium for most of the epochs while DM-SM number changing interactions remain out of equilibrium throughout. Only the number conserving scattering process $\text{DM } e \rightarrow \text{DM } e$, responsible for keeping both the dark and visible sectors in kinetic equilibrium, decouples around $x \sim 0.005$. Subsequently the temperature of the dark sector (denoted by T') evolves independently of the thermal bath (temperature T) until $x \sim 100$ when all the dark sector particles including light vector boson become non-relativistic and no longer contribute to the entropy degrees of freedom. Between these two epochs of DM-SM and dark sector decoupling, the ratio of the visible and dark sector temperatures can be obtained by conserving the total entropy separately in the two sectors. Considering the kinetic decoupling temperature to be T_D , we can relate the

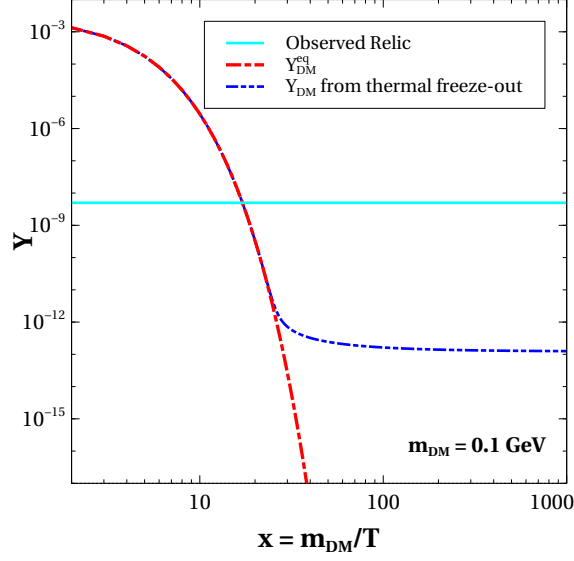


FIG. 6: Relic abundance of DM assuming it to be produced thermally in the early universe followed by thermal freeze-out. The thermal relic is under-abundant by two orders of magnitudes.

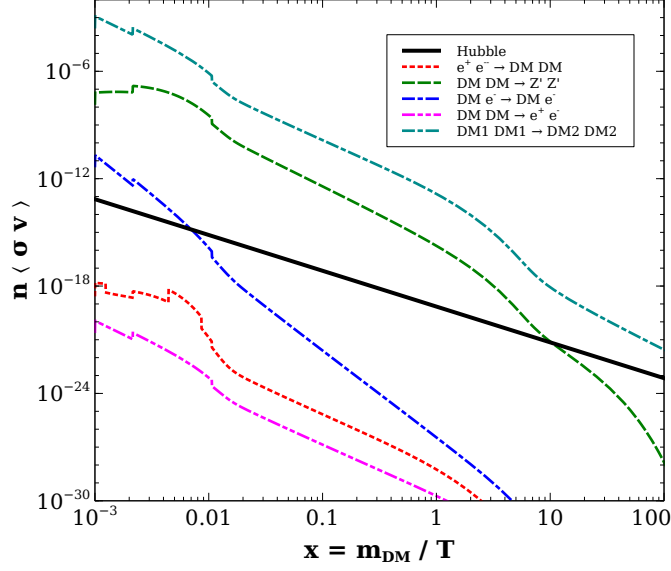


FIG. 7: Comparison of different scattering processes involving DM with Hubble rate of expansion.

temperature of the two sectors as

$$\frac{T'}{T} = \left(\frac{g_{*s}^{\text{SM}}(T)}{g_{*s}^{\text{SM}}(T_D)} \right)^{1/3}. \quad (11)$$

Here $g_{*s}^{\text{SM}}(T)$ is the relativistic entropy degrees of freedom in the SM which goes into the calculation of relativistic entropy density $s(T) = \frac{2\pi^2}{45} g_{*s}(T) T^3$. Since the above relation between two temperatures (11) is valid for $T < T_D$, we naturally have $g_{*s}^{\text{SM}}(T) < g_{*s}^{\text{SM}}(T_D)$

leading to $T' < T$. This is also understood from the fact that SM bath temperature receives additional entropy contributions from the species which keep getting decoupled gradually. Within the decoupled dark sector itself, the DM particles can transfer their entropy into lighter Z' bosons once T' falls below DM mass. This corresponds to an enhancement of dark sector temperature for $T' < m_{\text{DM}}$ by $(13/6)^{1/3}$, a factor close to unity. We have ignored this additional but tiny enhancement in the numerical calculations to be discussed below. For dark sector temperature, we can similarly define a dimensionless integration variable x' , related to the usual variable x as

$$x' = \frac{m_{\text{DM}}}{T'} = \left(\frac{T}{T'}\right)x. \quad (12)$$

Since we have two singlet fermions $\chi_{1,2}$ with tiny mass difference, identical gauge couplings and a strong $\chi_1\chi_1 \rightarrow \chi_2\chi_2$ conversion rate via Φ_2 exchange (required for boosted DM phenomenology to be discussed in upcoming section), we need to solve relevant Boltzmann equations for both of them. Additionally, as thermal relic of both $\chi_{1,2}$ will be sub-dominant due to large annihilation rates into Z' pairs, we consider an additional singlet scalar Φ_1 whose late decay can fill this deficit. Therefore, for a complete numerical analysis of DM relic abundance we need to solve three coupled Boltzmann equations for $\chi_{1,2}$ and Φ_1 . Unlike $\chi_{1,2}$ whose interactions with the SM bath are suppressed due to tiny kinetic mixing, the scalar singlet can be in thermal equilibrium with the SM due to large quartic couplings leading to thermal freeze-out followed by late decay into DM³. Defining the comoving number densities of these particles as $Y_{\chi_{1,2}} = n_{\chi_{1,2}}/s'(T'(T))$, $Y_{\Phi_1} = n_{\Phi_1}/s(T)$, the relevant coupled Boltzmann equations can be written as follows.

³ Similar hybrid setup can also be found in earlier works, for example, [79–83].

$$\begin{aligned}
\frac{dY_{\Phi_1}}{dx} &= -\frac{s(m_{\text{DM}})}{x^2 H(m_{\text{DM}}) \left(\frac{T'}{T}\right)} \langle \sigma(\Phi_1 \Phi_1 \rightarrow \text{SM SM}) v \rangle (Y_{\Phi_1}^2 - (Y_{\Phi_1}^{\text{eq}})^2) \\
&\quad - \frac{x \left(\frac{T'}{T}\right)^2}{H(m_{\text{DM}})} (\langle \Gamma_{\Phi_1 \rightarrow \chi_1 \chi_1} \rangle + \langle \Gamma_{\Phi_1 \rightarrow \chi_2 \chi_2} \rangle) Y_{\Phi_1}; \\
\frac{dY_{\chi_1}}{dx} &= \left(\frac{T'}{T}\right)^2 \left[\frac{s(m_{\text{DM}})}{x^2 H(m_{\text{DM}})} \left(\langle \sigma(e^+ e^- \rightarrow \chi_1 \chi_1) v \rangle (Y_{\chi_1}^{\text{eq}})^2 - \langle \sigma(\chi_1 \chi_1 \rightarrow Z' Z') v \rangle Y_{\chi_1}^2 \right. \right. \\
&\quad \left. \left. - \langle \sigma(\chi_1 \chi_1 \rightarrow \chi_2 \chi_2) v \rangle \left(Y_{\chi_1}^2 - \frac{(Y_{\chi_1}^{\text{eq}})^2}{(Y_{\chi_2}^{\text{eq}})^2} Y_{\chi_2}^2 \right) \right) + \frac{x \left(\frac{g_{*s}(T_D)}{g'_{*s}(T_D)}\right)}{H(m_{\text{DM}})} \langle \Gamma_{\Phi_1 \rightarrow \chi_1 \chi_1} \rangle Y_{\Phi_1} \right]; \\
\frac{dY_{\chi_2}}{dx} &= \left(\frac{T'}{T}\right)^2 \left[\frac{s(m_{\text{DM}})}{x^2 H(m_{\text{DM}})} \left(\langle \sigma(e^+ e^- \rightarrow \chi_2 \chi_2) v \rangle (Y_{\chi_1}^{\text{eq}})^2 - \langle \sigma(\chi_2 \chi_2 \rightarrow Z' Z') v \rangle Y_{\chi_2}^2 \right. \right. \\
&\quad \left. \left. + \langle \sigma(\chi_1 \chi_1 \rightarrow \chi_2 \chi_2) v \rangle \left(Y_{\chi_1}^2 - \frac{(Y_{\chi_1}^{\text{eq}})^2}{(Y_{\chi_2}^{\text{eq}})^2} Y_{\chi_2}^2 \right) \right) + \frac{x \left(\frac{g_{*s}(T_D)}{g'_{*s}(T_D)}\right)}{H(m_{\text{DM}})} \langle \Gamma_{\Phi_1 \rightarrow \chi_2 \chi_2} \rangle Y_{\Phi_1} \right]
\end{aligned} \tag{13}$$

where, $x = \frac{m_{\text{DM}}}{T}$, $s(m_{\text{DM}}) = \frac{2\pi^2}{45} g_{*S} m_{\text{DM}}^3$, $H(m_{\text{DM}}) = 1.67 g_*^{1/2} \frac{m_{\text{DM}}^2}{M_{\text{Pl}}}$ and $\langle \sigma(\Phi_1 \Phi_1 \rightarrow \text{SM SM}) v \rangle$ represents the thermally averaged cross-section [84] of annihilation of Φ_1 to all SM particles. The relevant cross-sections and decay widths are given in appendix A. Also, as mentioned earlier, $m_{\text{DM}} = m_{\chi_1} \approx m_{\chi_2}$. Note that the total Φ_1 decay width (Γ_{Φ_1}) is assumed to be very small leading to conversion of Φ_1 into DM at a late epoch, nevertheless well before the big bang nucleosynthesis (BBN). In fact, the chosen decay ($\Gamma_{\Phi_1} = 8.8 \times 10^{-23}$ GeV) corresponds to a lifetime of approximately 6.4×10^{-3} s.

Since SM and DM sectors evolve with different temperatures after a certain epoch, we accordingly divide the range of our numerical integration into two parts namely, (i) $x < 0.005$ where both the dark and the visible sectors share the same temperature $T = T'$, (ii) $0.005 < x < 100$ where the dark sector is decoupled from the visible sector ($T \neq T'$) and dark sector temperature (T') evolves according to (11). The evolution of these comoving number densities are shown in Fig. 8. To understand the importance of different processes in the Boltzmann equations, we show DM generation incorporating different annihilation or decay processes separately. For example, the red dashed line shows the freeze-in of DM⁴ from the SM bath (electrons, for example) without incorporating subsequent DM annihilations.

⁴ See [85, 86] for freeze-in DM details.

While DM abundance from freeze-in is huge compared to observed relic, incorporating DM annihilations lead to much smaller DM relic, shown by the pink dashed line. DM density further gets depleted due to large dark sector annihilation followed by an epoch where DM maintains equilibrium within dark sector. This is followed by a dark sector freeze-out around $x \sim 10$ leaving a saturated but suppressed DM relic shown by the pink dashed line. On the other hand, the singlet scalar Φ_1 can be produced in equilibrium due to large Higgs portal interactions. While the green dashed line shows its equilibrium distribution, the blue dashed line indicates the evolution after it freezes out from the bath, leaving a sizeable relic. At late epochs (after DM freezes out from the dark sector $x \sim 10$), the scalar singlet decays into DM filling the deficit as shown by the cyan dashed line. The singlet scalar abundance including its late decay is shown by the orange line. Since both the singlet fermions $\chi_{1,2}$ have same gauge coupling and tiny mass splitting, they get generated in almost equal amount from the bath and consequently from dark freeze-out. For simplicity we consider that Φ_1 decays only to χ_1 under the assumption of $y_2 \ll y_1$. However the strong inter-conversion $\chi_1\chi_1 \rightarrow \chi_2\chi_2$ with $\sigma(\chi_1\chi_1 \rightarrow \chi_2\chi_2) \sim 10^{-24}\text{cm}^2$, identical gauge interactions and tiny mass splitting lead to almost equal final relic of $\chi_{1,2}$. It is worth mentioning that even if Φ_1 decays to both $\chi_{1,2}$ equally, it does not affect the final relic significantly due to tiny mass splitting between them and in that case also $\chi_{1,2}$ will be equally abundant. This is in sharp contrast with other boosted DM scenarios, for example [58], where different final abundances of two DM fermions were found due to their different gauge interactions. Note that the decay of Φ_2 does not significantly affect the relic since the Yukawa coupling y' (see model Lagrangian 1) is large ($y' \sim \mathcal{O}(10^{-1})$) and hence Φ_2 decays to $\chi_{1,2}$ much before $\chi_{1,2}$ undergoes dark freeze-out. Any such initial abundance of DM will eventually get diluted due to strong annihilation into light mediator (Z') and the correct relic can only be obtained with late decay of Φ_1 .

V. BOOSTED DARK MATTER AND XENON1T EXCESS

The DM interpretation of the XENON1T excess with conventional dark matter is not possible, essentially because of its non-relativistic nature. For DM sufficiently heavier than the electron, the of electron recoil (kinetic) energy lies in a range of $\mathcal{O}(\text{eV})$ (*i.e.* $E_r \sim m_e \times (10^{-3}c)^2 \simeq \mathcal{O}(\text{eV})$ where m_e is mass of electron and $v \sim 10^{-3}c$ being the typical velocity of cold dark matter). On the other hand, XENON1T collaboration has reported

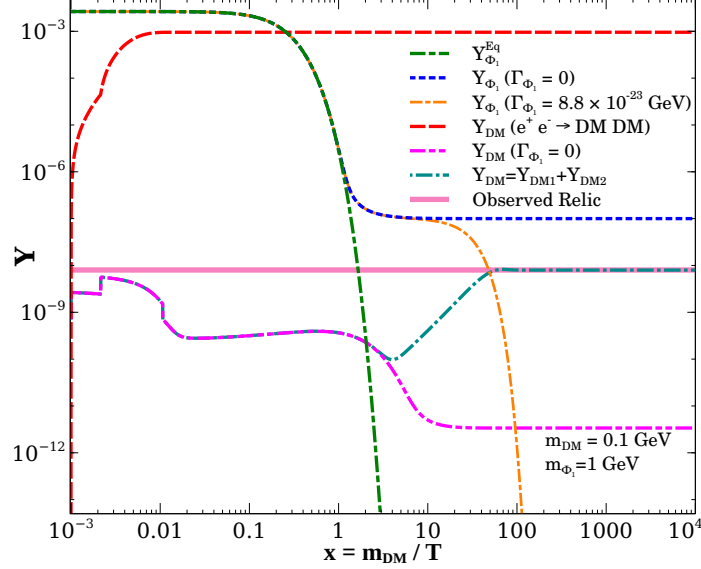


FIG. 8: Comoving number densities of dark sector particles considering different sub-processes indicated in the legends.

an excess of electron recoil events over the background in the recoil energy E_r in a range 1-7 keV, peaked around 2.4 keV [24]. This essentially implies that the energy deposition by conventional non-relativistic DM can not explain the excessive events of $\mathcal{O}(keV)$ as reported by the XENON1T collaboration. However, in scenarios involving a mechanism to exert sufficient boost onto a DM component, it is possible to explain the XENON1T excess through the elastic scattering of the boosted DM component off electron at the XENON1T detector.

In this boosted DM approach to explain the XENON1T excess, DM χ_1 which contributes to half of the total DM density in the present universe annihilates into dark matter χ_2 giving a significant boost to explain the reported excess. For a fixed incoming velocity v of DM fermion, the differential scattering cross-section for the elastic scattering process $\chi_2 e \rightarrow \chi_2 e$ can be written as

$$\frac{d\langle\sigma v\rangle}{dE_r} = \frac{\sigma_e}{2m_e v} \int_{q-}^{q+} a_0^2 q dq |F(q)|^2 K(E_r, q), \quad (14)$$

where m_e is the electron mass, σ_e is the corresponding free electron cross section at fixed momentum transfer $q = 1/a_0$ with $a_0 = \frac{1}{\alpha m_e}$ being the Bohr radius, $\alpha = \frac{e^2}{4\pi} = \frac{1}{137}$ being the fine structure constant, E_r is the recoil energy of electron and $K(E_r, q)$ is the atomic excitation factor. For our calculations, we adopt the the atomic excitation factor from [87] and we assume the DM fermion form factor to be unity. The dependency of atomic excitation

factor on the transferred momentum q is shown in Fig. 9. Here, the dominant contribution comes from the bound states with principal quantum number $n = 3$ as their binding energy is around a few keVs.

The free electron scattering cross-section for the process $\chi_2 e \rightarrow \chi_2 e$ is given by

$$\sigma_e = \frac{g'^2 \epsilon^2 g^2 m_e^2}{\pi M_{Z'}^4} \quad (15)$$

where ϵ is the kinetic mixing parameter between Z and Z' gauge bosons, g is the weak gauge coupling and g' is the $U(1)_D$ gauge coupling. As already mentioned, for DM sufficiently heavier than electron, the recoil cross-section σ_e is independent of DM mass as the reduced mass is almost equal to electron mass.

From the kinematics of the elastic scattering, the limits of integration for Eq. (14) are given by

$$q_{\pm} = m_{\chi_2} v \pm \sqrt{m_{\chi_2}^2 v^2 - 2m_{\chi_2} E_r}. \quad (16)$$

The differential event rate for the scattering of χ_2 with electrons in Xenon atom at XENON1T detector, *i.e* $\chi_2 e \rightarrow \chi_2 e$, can then be written as

$$\frac{dR}{dE_r} = n_T \Phi_{\chi_2} \frac{d\langle\sigma v\rangle}{dE_r} \quad (17)$$

where $n_T = 4 \times 10^{27} \text{ Ton}^{-1}$ is the number density of Xenon atoms and Φ_{χ_2} is the flux of the boosted χ_2 particle.

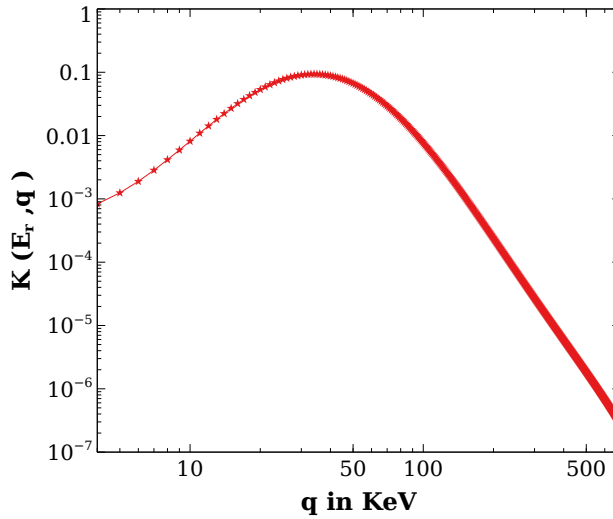


FIG. 9: Atomic excitation factor is shown as a function of momentum transferred.

In the present universe χ_1 can be assumed to annihilate to χ_2 only in DM dense regions like the Galactic center (GC) or the Sun⁵. If we consider the GC to be the source of boosted χ_2 (via the annihilation of the χ_1 with annihilation cross-section of order $\mathcal{O}(10^{-24} \text{ cm}^2)$, then the obtained flux is

$$\Phi_{\chi_2}^{\text{GC}} = 7.5 \times 10^9 \text{ cm}^{-2}\text{s}^{-1} \left(\frac{\langle \sigma_{\chi_1\chi_1 \rightarrow \chi_2\chi_2} v \rangle}{10^{-24} \text{ cm}^2} \right) \left(\frac{0.1 \text{ GeV}}{m_{\chi_1}} \right)^2 \quad (18)$$

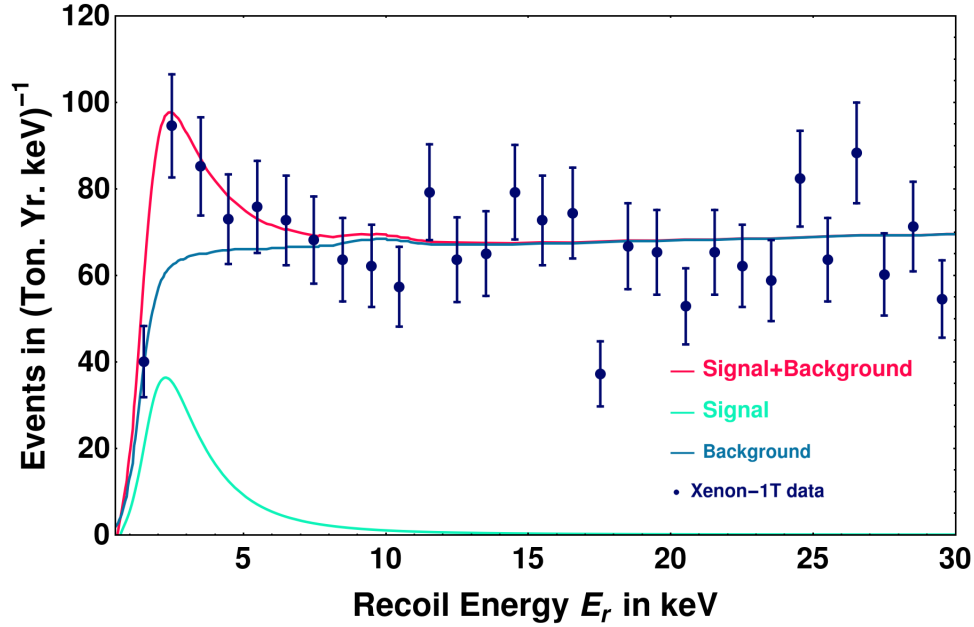


FIG. 10: Fit to XENON1T electron recoil excess with the Boosted dark matter

The final detected recoil energy spectrum can be obtained by convolving Eq. (17) with the energy resolution of the XENON1T detector. Incorporating the detector efficiency $\gamma(E)$, the energy resolution of the detector is given by a Gaussian distribution with an energy dependent width,

$$\zeta(E, E_r) = \frac{1}{\sqrt{2\pi\sigma_{\text{det}}^2}} \text{Exp} \left[-\frac{(E - E_r)^2}{2\sigma_{\text{det}}^2} \right] \times \gamma(E) \quad (19)$$

⁵ In the case of boosted flux from the Sun, strong evaporation bound [88, 89] forces us to choose DM mass in the GeV regime where DM-nucleon scattering rate faces tight constraints from direct search experiments like CRESST-III [90]. Thus, the required χ_2 flux from solar captured χ_1 can not be obtained.

where $\gamma(E)$ is reported in Fig. 2 of [24] and the width σ_{det} is given by

$$\sigma_{\text{det}}(E) = a\sqrt{E} + bE \quad (20)$$

with $a = 0.3171$ and $b = 0.0037$. Thus the final detected recoil energy spectrum is given by

$$\frac{dR_{\text{det}}}{dE_r} = \frac{n_T \Phi_{\chi_2} \sigma_e a_0^2}{2m_e v} \int dE \quad \zeta(E, E_r) \left[\int_{q^-}^{q^+} dq \quad q \quad K(E_r, q) \right] \quad (21)$$

With the flux mentioned in Eq.(18), the electron scattering cross-section σ_e that can explain the electron recoil excess at XENON1T is calculated to be $1.5 \times 10^{-15} \text{ GeV}^{-2}$. To obtain the fit to XENON1T data shown in Fig. 10 we have used benchmark values $m_{\chi_2} = 0.099875 \text{ GeV}$, $v = 0.05$. Such velocities can be obtained by fixing $\Delta m/m_{\chi_2} = 1.25 \times 10^{-3}$ where $\Delta m = m_{\chi_1} - m_{\chi_2}$ giving rise to the necessary boost factor.

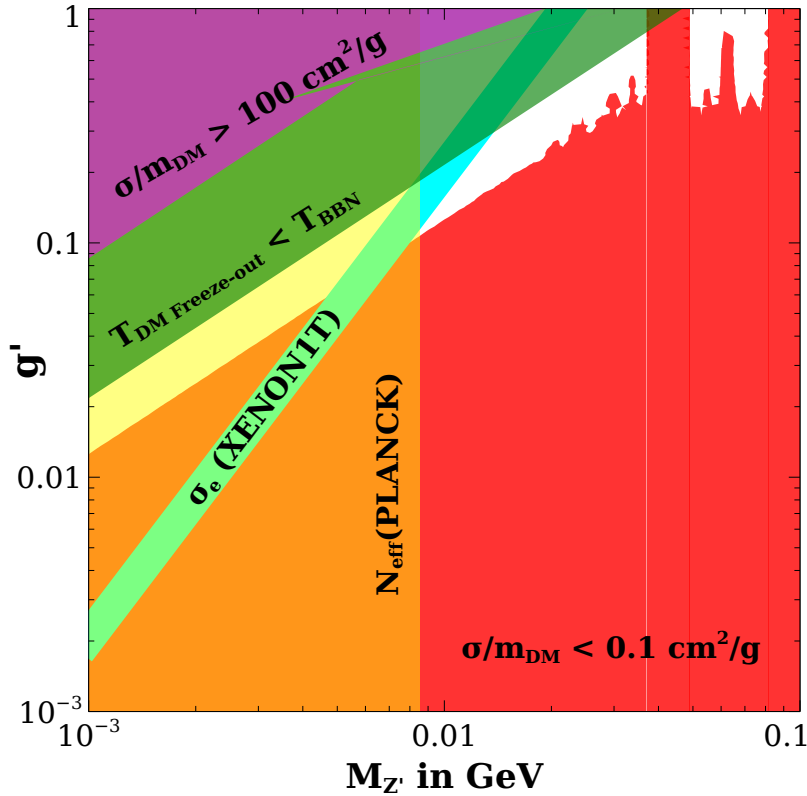


FIG. 11: Summary plot showing the parameter space in $g' - M_{Z'}$ plane considering kinetic mixing parameter $\epsilon = 10^{-7}$ and DM mass $m_{\text{DM}} = 0.1 \text{ GeV}$.

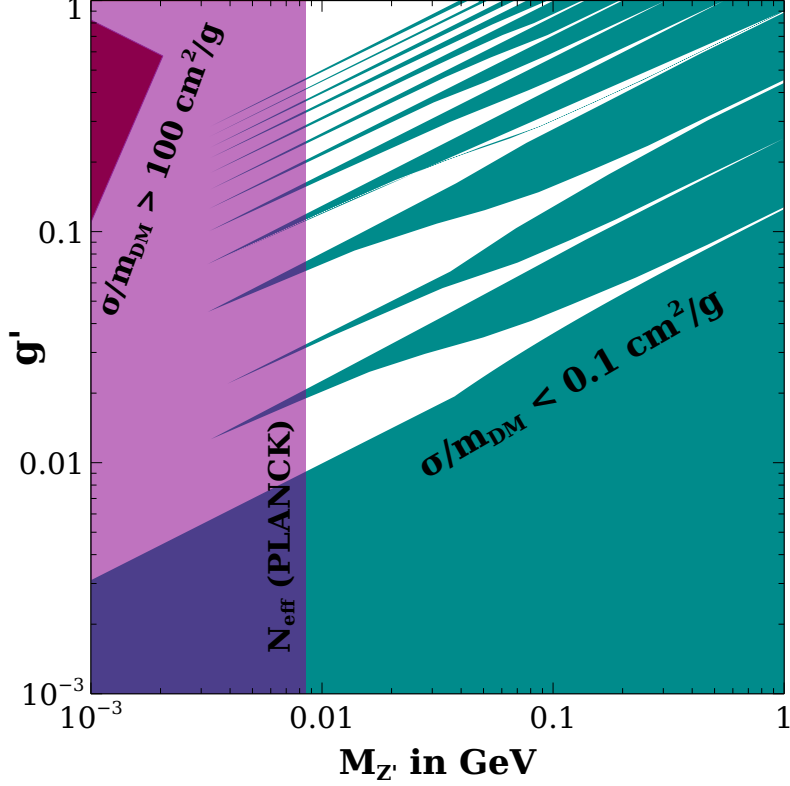


FIG. 12: Summary plot showing the parameter space in $g' - M_{Z'}$ plane considering kinetic mixing parameter $\epsilon = 10^{-7}$ and DM mass $m_{\text{DM}} = 100$ GeV.

VI. CONCLUSION

We have proposed a boosted self-interacting dark matter scenario as a possible origin of XENON1T electron excess. Adopting a minimal scenario where DM is composed of two vector like singlet fermions charged under a dark Abelian gauge symmetry. While sufficient DM self-interactions can be generated due to the existence of light vector boson, the XENON1T excess can be realised from boosted component of DM scattering off electrons. Sufficient boost factor can be realised by tuning the mass splitting between two DM fermions and the cross section of their inter-conversion. While DM can be produced from the thermal bath via freeze-in mechanism due to tiny kinetic mixing of neutral vector bosons, the final abundance remains suppressed due to large DM annihilation rates within dark sector. The deficit can be filled through late decay of a singlet scalar which freezes out earlier from the thermal bath. Adopting suitable benchmark values, we have shown how correct relic of DM can be generated by solving the coupled Boltzmann equations involving two DM fermions

as well as the late decaying single scalar. We have also shown how XENON1T data can be fitted by boosted SIDM in this scenario.

In Fig. 11, we summarise the final parameter space in $g' - M_{Z'}$ plane considering DM mass to be 0.1 GeV and kinetic mixing parameter $\epsilon = 10^{-7}$. The upper left and lower right regions are disfavoured as they give rise to too large and too small DM self-interactions respectively, leaving a band in between. From this band also, more than half of the region is disfavoured from the criteria of DM freeze-out happening before the BBN epochs. Although, by DM freeze-out we mean DM freezing out within dark sector only where DM annihilates primarily into each other or light vector boson Z' , eventually, Z' will decay into SM particles via kinetic mixing as it can not decay into DM kinematically. Therefore, as a conservative bound, we impose the criteria of DM freeze-out temperature to be more than BBN temperature. Very light Z' is ruled out from cosmological constraints on effective relativistic degrees of freedom [2, 91–93]. This arises due to the late decay of such light gauge bosons into SM leptons, after standard neutrino decoupling temperatures thereby enhancing N_{eff} . The corresponding disfavoured region is shaded in orange colour. Thus, only the thin white coloured region on upper right half of the plane remains allowed from these criteria. Since we are considering tiny kinetic mixing, the direct detection bounds from CRESST-III [90] do not apply in this plane. The cyan coloured band denotes the required $\chi_2 - e$ scattering cross section to give rise to the XENON1T fit. Clearly, only a tiny triangular region remains allowed from all these criteria, keeping the model very predictive and verifiable at near future experiments. It is noteworthy that, we are not incorporating DM relic constraints in this plane as those can be satisfied independently by appropriate tuning of singlet scalar couplings. It should be noted that we have chosen light sub-GeV DM in order to get the desired boosted DM flux as well as DM-electron scattering without conflicting other existing bounds. This has led to very tiny allowed region of parameter space. To make this point clear, we also show another summary plot in Fig. 12 by considering DM mass to be 100 GeV. Clearly we have more allowed region of parameter space although XENON1T fit is not possible in such a scenario. While we have confined ourselves to the discussion of DM aspects only in this work, such dark $U(1)_D$ gauge symmetry can also have consequences for the origin of light neutrino mass [37], flavour anomalies [94], as well as cosmological phase transitions and gravitational waves [95]. We leave such interesting aspects of $U(1)_D$ gauge symmetry to future studies.

Acknowledgments

DB acknowledges the support from Early Career Research Award from Science and Engineering Research Board (SERB), Department of Science and Technology (DST), Government of India (reference number: ECR/2017/001873). MD acknowledges DST, Government of India for providing the financial assistance for the research under the grant DST/INSPIRE/03/ 2017/000032.

Appendix A: Relevant cross section and decay widths

$$\Gamma(\Phi_1 \rightarrow \chi_1 \chi_1) = \frac{y_1^2}{8\pi} m_{\Phi_1} \left(1 - 4 \frac{m_{\chi_1}^2}{m_{\Phi_1}^2}\right)^{3/2} \quad (\text{A1})$$

$$\sigma(\chi_1 \chi_1 \rightarrow \chi_2 \chi_2) = \frac{y_1'^2 y_2'^2}{32\pi s} \frac{(s - 4m_{\chi_2}^2)^{3/2} (s - 4m_{\chi_1}^2)^{1/2}}{(s - m_{\Phi_2}^2)^2} \quad (\text{A2})$$

$$\begin{aligned} \sigma(\chi \chi \rightarrow Z' Z') &= \frac{g'^4}{192\pi s(s - 4m_\chi^2)} \times \left[\frac{24s(4m_\chi^4 + 2M_{Z'}^4 + sm_\chi^2)A}{M_{Z'}^4 + m_\chi^2 s - 4M_{Z'}^2 m_\chi^2} \right. \\ &\quad \left. - \frac{24(8m_\chi^2 - 4M_{Z'}^2 - s^2 - (s - 2M_{Z'}^2)4m_\chi^2)}{s - 2M_{Z'}^2} \text{Log} \left[\frac{2M_{Z'}^2 + s(A - 1)}{2M_{Z'}^2 - s(A + 1)} \right] \right] \end{aligned} \quad (\text{A3})$$

where $A = \sqrt{\frac{(s - 4M_{Z'}^2)(s - 4m_\chi^2)}{s^2}}$

$$\sigma(e^+ e^- \rightarrow \chi \chi) = \frac{g^2 g'^2 \epsilon^2 (s + 2m_\chi^2)(s - m_e^2 - 4(s + 2m_e^2) \sin^2 \theta_W)}{96\pi \cos^2 \theta_W (s - 4m_e^2)(s - m_{Z'}^2)^2} \sqrt{\frac{(s - 4m_e^2)(s - 4m_\chi^2)}{s^2}} \quad (\text{A4})$$

Thermal averaged cross-section for annihilation of any particle A to B is given by: [84]

$$\langle \sigma v \rangle_{AA \rightarrow BB} = \frac{x}{2[K_1^2(x) + K_2^2(x)]} \times \int_2^\infty dz \sigma_{(AA \rightarrow BB)}(z^2 m_A^2)(z^2 - 4)z^2 K_1(zx) \quad (\text{A5})$$

where $z = \sqrt{s}/m_A$ and $x = m_A/T$.

Thermal averaged decay width of Φ_1 decaying to χ_1 is given by:

$$\langle \Gamma(\Phi_1 \rightarrow \chi_1 \chi_1) \rangle = \Gamma(\Phi_1 \rightarrow \chi_1 \chi_1) \left(\frac{K_1(x)}{K_2(x)} \right) \quad (\text{A6})$$

In Eqn. (A5) and (A6), K_1 and K_2 are the modified Bessel functions of 1st and 2nd kind respectively.

-
- [1] P. A. Zyla et al. (Particle Data Group), PTEP **2020**, 083C01 (2020).
 - [2] N. Aghanim et al. (Planck) (2018), 1807.06209.
 - [3] F. Zwicky, Helv. Phys. Acta **6**, 110 (1933), [Gen. Rel. Grav.41,207(2009)].
 - [4] V. C. Rubin and W. K. Ford, Jr., Astrophys. J. **159**, 379 (1970).
 - [5] D. Clowe, M. Bradac, A. H. Gonzalez, M. Markevitch, S. W. Randall, C. Jones, and D. Zaritsky, Astrophys. J. **648**, L109 (2006), astro-ph/0608407.
 - [6] E. W. Kolb and M. S. Turner, *The Early Universe*, vol. 69 (1990), ISBN 978-0-201-62674-2.
 - [7] G. Arcadi, M. Dutra, P. Ghosh, M. Lindner, Y. Mambrini, M. Pierre, S. Profumo, and F. S. Queiroz (2017), 1703.07364.
 - [8] S. Tulin and H.-B. Yu, Phys. Rept. **730**, 1 (2018), 1705.02358.
 - [9] J. S. Bullock and M. Boylan-Kolchin, Ann. Rev. Astron. Astrophys. **55**, 343 (2017), 1707.04256.
 - [10] D. N. Spergel and P. J. Steinhardt, Phys. Rev. Lett. **84**, 3760 (2000), astro-ph/9909386.
 - [11] A. A. de Laix, R. J. Scherrer, and R. K. Schaefer, Astrophys. J. **452**, 495 (1995), astro-ph/9502087.
 - [12] M. R. Buckley and P. J. Fox, Phys. Rev. D **81**, 083522 (2010), 0911.3898.
 - [13] J. L. Feng, M. Kaplinghat, and H.-B. Yu, Phys. Rev. Lett. **104**, 151301 (2010), 0911.0422.
 - [14] J. L. Feng, M. Kaplinghat, H. Tu, and H.-B. Yu, JCAP **07**, 004 (2009), 0905.3039.
 - [15] A. Loeb and N. Weiner, Phys. Rev. Lett. **106**, 171302 (2011), 1011.6374.
 - [16] J. Zavala, M. Vogelsberger, and M. G. Walker, Mon. Not. Roy. Astron. Soc. **431**, L20 (2013), 1211.6426.
 - [17] M. Vogelsberger, J. Zavala, and A. Loeb, Mon. Not. Roy. Astron. Soc. **423**, 3740 (2012), 1201.5892.
 - [18] T. Bringmann, F. Kahlhoefer, K. Schmidt-Hoberg, and P. Walia, Phys. Rev. Lett. **118**, 141802 (2017), 1612.00845.
 - [19] M. Kaplinghat, S. Tulin, and H.-B. Yu, Phys. Rev. Lett. **116**, 041302 (2016), 1508.03339.
 - [20] L. G. van den Aarssen, T. Bringmann, and C. Pfrommer, Phys. Rev. Lett. **109**, 231301 (2012),

1205.5809.

- [21] S. Tulin, H.-B. Yu, and K. M. Zurek, Phys. Rev. D **87**, 115007 (2013), 1302.3898.
- [22] M. Kaplinghat, S. Tulin, and H.-B. Yu, Phys. Rev. D **89**, 035009 (2014), 1310.7945.
- [23] E. Del Nobile, M. Kaplinghat, and H.-B. Yu, JCAP **10**, 055 (2015), 1507.04007.
- [24] E. Aprile et al. (XENON) (2020), 2006.09721.
- [25] F. Takahashi, M. Yamada, and W. Yin, Phys. Rev. Lett. **125**, 161801 (2020), 2006.10035.
- [26] G. Alonso-Álvarez, F. Ertas, J. Jaeckel, F. Kahlhoefer, and L. J. Thormaehlen (2020), 2006.11243.
- [27] K. Kannike, M. Raidal, H. Veermäe, A. Strumia, and D. Teresi (2020), 2006.10735.
- [28] B. Fornal, P. Sandick, J. Shu, M. Su, and Y. Zhao, Phys. Rev. Lett. **125**, 161804 (2020), 2006.11264.
- [29] M. Du, J. Liang, Z. Liu, V. Q. Tran, and Y. Xue (2020), 2006.11949.
- [30] P. Ko and Y. Tang (2020), 2006.15822.
- [31] L. Su, W. Wang, L. Wu, J. M. Yang, and B. Zhu (2020), 2006.11837.
- [32] K. Harigaya, Y. Nakai, and M. Suzuki (2020), 2006.11938.
- [33] D. Borah, S. Mahapatra, D. Nanda, and N. Sahu (2020), 2007.10754.
- [34] D. Choudhury, S. Maharana, D. Sachdeva, and V. Sahdev (2020), 2007.08205.
- [35] J. Bramante and N. Song, Phys. Rev. Lett. **125**, 161805 (2020), 2006.14089.
- [36] N. F. Bell, J. B. Dent, B. Dutta, S. Ghosh, J. Kumar, and J. L. Newstead, Phys. Rev. Lett. **125**, 161803 (2020), 2006.12461.
- [37] D. Borah, S. Mahapatra, and N. Sahu (2020), 2009.06294.
- [38] A. Aboubrahim, M. Klasen, and P. Nath (2020), 2011.08053.
- [39] H. M. Lee (2020), 2006.13183.
- [40] S. Baek, J. Kim, and P. Ko, Phys. Lett. B **810**, 135848 (2020), 2006.16876.
- [41] S. Shakeri, F. Hajkarim, and S.-S. Xue, Journal of High Energy Physics **2020** (2020), ISSN 1029-8479, URL [http://dx.doi.org/10.1007/JHEP12\(2020\)194](http://dx.doi.org/10.1007/JHEP12(2020)194).
- [42] A. Bally, S. Jana, and A. Trautner, Phys. Rev. Lett. **125**, 161802 (2020), 2006.11919.
- [43] L. Delle Rose, G. Hütsi, C. Marzo, and L. Marzola (2020), 2006.16078.
- [44] Y. Ema, F. Sala, and R. Sato (2020), 2007.09105.
- [45] M. Dutta, S. Mahapatra, D. Borah, and N. Sahu (2021), 2101.06472.
- [46] M. Baryakhtar, A. Berlin, H. Liu, and N. Weiner (2020), 2006.13918.

- [47] W. Chao, Y. Gao, and M. j. Jin (2020), 2006.16145.
- [48] H. An and D. Yang (2020), 2006.15672.
- [49] H.-J. He, Y.-C. Wang, and J. Zheng (2020), 2007.04963.
- [50] J. Kim, T. Nomura, and H. Okada, Phys. Lett. B **811**, 135862 (2020), 2007.09894.
- [51] W.-Y. Keung, D. Marfatia, and P.-Y. Tseng (2020), 2009.04444.
- [52] H.-J. He, Y.-C. Wang, and J. Zheng (2020), 2012.05891.
- [53] S.-M. Choi, H. M. Lee, and B. Zhu (2020), 2012.03713.
- [54] D. McKeen, M. Pospelov, and N. Raj (2020), 2006.15140.
- [55] Y. Jho, J.-C. Park, S. C. Park, and P.-Y. Tseng (2020), 2006.13910.
- [56] H. Alhazmi, D. Kim, K. Kong, G. Mohlabeng, J.-C. Park, and S. Shin (2020), 2006.16252.
- [57] A. Das and M. Sen (2021), 2104.00027.
- [58] D. Borah, M. Dutta, S. Mahapatra, and N. Sahu (2021), 2104.05656.
- [59] H. Alhazmi, K. Kong, G. Mohlabeng, and J.-C. Park, Journal of High Energy Physics **2017** (2017), ISSN 1029-8479, URL [http://dx.doi.org/10.1007/JHEP04\(2017\)158](http://dx.doi.org/10.1007/JHEP04(2017)158).
- [60] J. Berger, Y. Cui, and Y. Zhao, Journal of Cosmology and Astroparticle Physics **2015**, 005–005 (2015), ISSN 1475-7516, URL <http://dx.doi.org/10.1088/1475-7516/2015/02/005>.
- [61] Y. Jho, J.-C. Park, S. C. Park, and P.-Y. Tseng, *Cosmic-neutrino-boosted dark matter (νbdm)* (2021), 2101.11262.
- [62] K. Kong, G. Mohlabeng, and J.-C. Park, Physics Letters B **743**, 256–266 (2015), ISSN 0370-2693, URL <http://dx.doi.org/10.1016/j.physletb.2015.02.057>.
- [63] K. Agashe, Y. Cui, L. Necib, and J. Thaler, Journal of Cosmology and Astroparticle Physics **2014**, 062–062 (2014), ISSN 1475-7516, URL <http://dx.doi.org/10.1088/1475-7516/2014/10/062>.
- [64] S. Baek (2021), 2105.00877.
- [65] D. Kim, J.-C. Park, and S. Shin, Phys. Rev. Lett. **119**, 161801 (2017), 1612.06867.
- [66] G. F. Giudice, D. Kim, J.-C. Park, and S. Shin, Phys. Lett. B **780**, 543 (2018), 1712.07126.
- [67] S. Tulin, H.-B. Yu, and K. M. Zurek, Phys. Rev. Lett. **110**, 111301 (2013), 1210.0900.
- [68] S. A. Khrapak, A. V. Ivlev, G. E. Morfill, and S. K. Zhdanov, Phys. Rev. Lett. **90**, 225002 (2003).
- [69] A. Kamada, H. J. Kim, and T. Kuwahara, JHEP **20**, 202 (2020), 2007.15522.
- [70] C. Kouvaris, I. M. Shoemaker, and K. Tuominen, Phys. Rev. D **91**, 043519 (2015), 1411.3730.

- [71] N. Bernal, X. Chu, C. Garcia-Cely, T. Hambye, and B. Zaldivar, JCAP **03**, 018 (2016), 1510.08063.
- [72] K. Kainulainen, K. Tuominen, and V. Vaskonen, Phys. Rev. D **93**, 015016 (2016), [Erratum: Phys.Rev.D 95, 079901 (2017)], 1507.04931.
- [73] T. Hambye and L. Vanderheyden, JCAP **05**, 001 (2020), 1912.11708.
- [74] M. Cirelli, P. Panci, K. Petraki, F. Sala, and M. Taoso, JCAP **05**, 036 (2017), 1612.07295.
- [75] F. Kahlhoefer, K. Schmidt-Hoberg, and S. Wild, JCAP **08**, 003 (2017), 1704.02149.
- [76] G. Bélanger and J.-C. Park, Journal of Cosmology and Astroparticle Physics **2012**, 038–038 (2012), ISSN 1475-7516, URL <http://dx.doi.org/10.1088/1475-7516/2012/03/038>.
- [77] A. Semenov, Comput. Phys. Commun. **201**, 167 (2016), 1412.5016.
- [78] A. Belyaev, N. D. Christensen, and A. Pukhov, Comput. Phys. Commun. **184**, 1729 (2013), 1207.6082.
- [79] J. L. Feng, A. Rajaraman, and F. Takayama, Phys. Rev. **D68**, 063504 (2003), hep-ph/0306024.
- [80] D. Borah, D. Nanda, and A. K. Saha (2019), 1904.04840.
- [81] A. Biswas, D. Borah, and D. Nanda, JCAP **1809**, 014 (2018), 1806.01876.
- [82] D. Borah, B. Karmakar, and D. Nanda, JCAP **1807**, 039 (2018), 1805.11115.
- [83] D. Borah and A. Gupta, Phys. Rev. **D96**, 115012 (2017), 1706.05034.
- [84] P. Gondolo and G. Gelmini, Nucl. Phys. **B360**, 145 (1991).
- [85] L. J. Hall, K. Jedamzik, J. March-Russell, and S. M. West, JHEP **03**, 080 (2010), 0911.1120.
- [86] N. Bernal, M. Heikinheimo, T. Tenkanen, K. Tuominen, and V. Vaskonen, Int. J. Mod. Phys. **A32**, 1730023 (2017), 1706.07442.
- [87] B. Roberts and V. Flambaum, Phys. Rev. D **100**, 063017 (2019), 1904.07127.
- [88] K. Griest and D. Seckel, Nucl. Phys. B **283**, 681 (1987), [Erratum: Nucl.Phys.B 296, 1034–1036 (1988)].
- [89] A. Gould, Astrophys. J. **321**, 560 (1987).
- [90] A. Abdelhameed et al. (CRESST), Phys. Rev. D **100**, 102002 (2019), 1904.00498.
- [91] A. Kamada, K. Kaneta, K. Yanagi, and H.-B. Yu, JHEP **06**, 117 (2018), 1805.00651.
- [92] M. Ibe, S. Kobayashi, Y. Nakayama, and S. Shirai, JHEP **04**, 009 (2020), 1912.12152.
- [93] M. Escudero, D. Hooper, G. Krnjaic, and M. Pierre, JHEP **03**, 071 (2019), 1901.02010.
- [94] Y.-D. Tsai, P. deNiverville, and M. X. Liu, Phys. Rev. Lett. **126**, 181801 (2021), 1908.07525.
- [95] D. Borah, A. Dasgupta, and S. K. Kang (2021), 2105.01007.